Electronic Supplementary Material (ESI) for ChemComm.

Supporting Information

MnO_x MFs as Coreaction Accelerator for Construction of a Novel Ternary Electrochemiluminescence System: Ultrasensitive Detection of MicroRNA

Rong Yang, Jia-Li Liu, Ya-Qin Chai* and Ruo Yuan*

Key Laboratory of Luminescent and Real-Time Analytical Chemistry (Southwest University), Ministry of Education, College of Chemistry and Chemical Engineering, Southwest University, Chongqing 400715, China.

* Corresponding authors.

E-mail addresses: yqchai@swu.edu.cn (Y. Q. Chai), yuanruo@swu.edu.cn (R. Yuan)

Table of Contents for Supporting Information

1. Experimental Section

1.1 Reagents and Apparatus.

Luminol, chitosan, 1-hexanethiol (HT), ferrocenecarboxylic acid (FcCOOH), *N*-hydroxysuccinimide (NHS) and *N*-(3-dimethylaminopropyl)-*N*-ethylcarbodiimide hydrochloride (EDC) were purchased from Sigma-Aldrich Co. (St. Louis, MO, USA). manganese sulfate ($MnSO_4•H_2O$), ammonium sulfate ($(NH_4)_2SO_4$) and sodium hydroxide (NaOH) were bought from Chengdu Kelong Chemical Industry (Chengdu, China). Ascorbic acid and polyvinylpyrrolidone (PVP) were obtained from Chemical Reagent Co. Ltd. (Chongqing, China). Silver nitrate ($AgNO_3$), chloroplatinic acid ($H_2PtCl_6•6H_2O$) were puchased from Sinopharm Chemical Reagent Co. Ltd. (Shanghai, China). Multi-walled carbon nanotubes (MWCNTs) were bought from Nanjing Xianfeng Nano Co. (Nanjing, China). Ammonium persulfate ($(NH_4)_2S_2O_8$), doxorubicin hydrochloride (Dox), microRNA-21 (purified by HPLC) and all DNA oligonucleotides (hairpin H1 ~ H4, purified by PAGE) were obtained from Sangon, Inc. (Shanghai, China). Phosphate-buffered solution (PBS, containing 0.1 M Na_2HPO_4, 0.1 KH_2PO_4 and 0.1 M KCl, NaOH and HCl were used to adjust the pH) was employed as the working buffer solution (pH 8.0) and rinse solution (pH7.4). 1 × TE buffer (10 mM Tris-HCl, 1.0 mM ethylenediaminetetraacetic acid (EDTA), pH 8.0) was used to dissolve and store all oligonucleotides. Tris-acetate-EDTA/Mg^{2+} buffer (TAE/Mg^{2+}) contained 40 mM Tris-HCl (pH 8.0), 20 mM acetic acid, 2 mM EDTA, 12.5 mM $MgCl_2$ was employed as hybridization buffer. Deionized water

(specific resistance of 18.2 MΩ•cm) was used throughout this experiment.

ECL emission was measured by a MPI-A multifunctional analyzer (Xi'An Remax Electronic Science & Technology Co. Ltd., Xi'An, China). Cyclic voltammetry (CV) experiment was carried out with CHI 660C Electrochemistry Workstation (Shanghai CH Instruments, China). Field emission scanning electron microscopies (SEM) were implemented on S-4800 and SU 8023 (Hitachi, Tokyo, Japan). Elemental mapping were performed on SU 8023 (Hitachi, Tokyo, Japan). High resolution transmission electron microscopy (HRTEM) and selected area electron diffraction (SAED) were obtained from Tecnai G2 F20 S-TWIN (FEI, Hillsboro, OR, USA) with an acceleration voltage of 200 kV. X-ray diffraction (XRD) measurement was investigated by D8 Advance X-ray diffractometer (Bruker, Stuttgart, Germany). X-ray photoelectron spectroscopy (XPS) was performed on 250Xi (Thermo Scientific Escalab, USA). Ultraviolet-visible (UV-vis) absorption spectra were measured with a UV-2450 UV-vis spectrophotometer (Shimadzu, Tokyo, Japan). Fluorescence spectra were recorded with a RF-5301PC spectrophotometer (Shimadzu, Tokyo, Japan). ECL emission spectra were studied with an electrochemical workstation combined with a Newton EMCCD spectroscopy detector (Andor Co., Tokyo, Japan). Native polyacrylamide gel electrophoresis was performed with a BG-verMIDI standard vertical electrophoresis apparatus (Baygene, China) and a Gel Doc XR+ System (Bio-Rad, USA). Three-electrode system employed in this work: glassy carbon electrode (GCE, Φ = 4 mm, bare or modified) as working electrode, Ag/AgCl (sat. KCl) electrode as reference electrode, platinum wire electrode as counter

electrode.

Table S1. Sequence Information for the Nucleic Acids Used in This Study

Name	Sequences (5′-3′)
miRNA-21	UAGCUUAUCAGACUGAUGUUGA
H1	NH_2- $(CH_2)_6$TCAACATCAGTCTGATAAGCTAGAATTCTTAACGTCGCCTG CCATACTGTAGCTTATCAGACTGA
H2	TAGCTTATCAGACTGATGTTGATCAGTCTGATAAGCTACAGTATG GCAACCTAGCAGAGTT
H3	TCGCCTCCTAGCAGAGTTACTTTGACCTGGAACTCTGCTAGGAGG CGACGTTAAGAATTC
H4	CCAGGTCAAAGTAACTCTGCTAGGAGGCGAGAATTCTTAACGTC GCCTCCTAGCAGAGTT

1.2 Gel Electrophoresis.

Polyacrylamide gel electrophoresis (PAGE) were operated to characterize the result of the hybridization chain reaction. All hairpins were heated at 95 °C for 5 min respectively and then cooled to room temperature before use. Nucleic acid samples were then injected into the lanes of freshly non-denaturing polyacrylamide gel (8%). Afterwards, electrophoresis was performed in 1 × TBE buffer at 120 V for 90 min. After dying with GelGreen, the gel was photographed by the Bio-Rad Gel Doc XR+ System (The PAGE images was showed in Fig. S7).

1.3 Synthesis of Luminol-MWCNTs@MnO_x MFs Composite (L-M@MnO_x MFs).

MnO_x MFs were synthesized according to literature with tiny modifications.[1]

First of all, 0.09 g $MnSO_4 \cdot H_2O$ and 0.175 g $(NH_4)_2SO_4$ were added into 15 mL of deionized water under magnetic stirring to form clear solution. Then, a total of 5 mL of $(NH_4)_2S_2O_8$ solution (0.12 g $(NH_4)_2S_2O_8$) was dropped into the above mixed solution under continuous stirring of several minutes. The prepared homogenous mixture solution was finally shifted to a Teflon-lined stainless steel autoclave, and heated to 70 ^oC for 9 h in a vacuum oven. Cooled down to room temperature, the black particles were collected through centrifugation and washed with deionized water for 3 times, then heated at 60 ^oC to obtain dry solid powder.

Carboxylated multi-walled carbon nanotubes (MWCNTs-COOH) were prepared via the typical acid treatment.[2] Briefly, 10 mg MWCNTs were dispersed in mixed acid solution of H_2SO_4 and HNO_3 (volume ratio 3:1) with reflux at boiling point for 40 min. After that, the black precipitates (MWCNTs-COOH) were washed until neutral and dried at 60 ^oC. For the preparation of MWCNTs@MnO_x MFs (M@MnO_x MFs), 10 mg MWCNTs-COOH and 40 mg MnO_x MFs were dispersed in 15 mL water, followed by ultrasonic treatment for 6 h to interwine the flower-like MnO_x MFs with tubular MWCNTs-COOH.

Ultimately, Luminol-MWCNTs@MnO_x MFs (L-M@MnO_x MFs) were fabricated by means of amide reaction. 1 mg as-prepared M@MnO_x MFs were added into 2 mL ultrapure water, and subsequently 0.3 mmol of EDC and 0.075 mmol of NHS were added into the suspension under gentle agitation to activate the carboxyls of MWCNTs-COOH for 0.5 h. Afterwards, 300 μL of 0.2 M luminol was dropped

into the above solution under continuous stirring for 4 h. Then, the obtained greyish and evenly dispersed suspension liquid was washed to eliminate residual unreacted substances. The obtained L-M@MnO_x MFs were dispersed into 1 mL deionized water and reserved in 4 ^oC refrigerator for future use.

1.4 Synthesis of Doxorubicin Ferrocenecarboxylic Acid Compound (Dox-FcCOOH).

The Dox-FcCOOH compound was synthesized through amide reaction (as depicted in Scheme S1). In detail, 0.6 mL of ferrocenecarboxylic acid (FcCOOH) ethanol solution (1 mM) was mingled with 0.5 mL of mixed solution containing 30 mM EDC and 7.5 mM NHS on a magnetic stirrer shielded from light. Half an hour later, 0.6 mL of doxorubicin hydrochloride solution (1.5 mM) was added into the above solution dropwise with a pipette. For full reaction, the above mixture was kept agitating for another 4 h to obtain the Dox-FcCOOH compound.

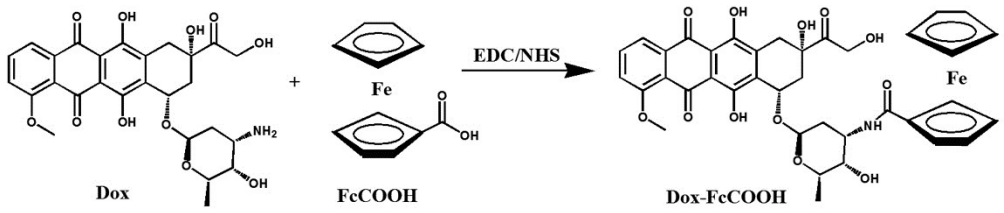

Scheme S1. Synthetic route of the Dox-FcCOOH compound.

1.5 Fabrication of AgPt Nanoparticles (AgPt NPs).

The synthetic steps of AgPt NPs were based on a previous study with minor amendments.[3] To begin with, 50 μL of 1 M NaOH solution, 3 mL of 10 mM fresh

ascorbic acid along with 50 mg polyvinylpyrrolidone (PVP) powder were successively added into 2 mL deionized water under ceaselessly stirring. Then, 4 mL of 2 mM $AgNO_3$ solution was dropped into the formed pellucid solution. After 20 min stirring, the solution turned brown, and 4 mL of 2 mM H_2PtCl_6 aqueous solution was added. Kept in a water bath of 60 ^oC, the mixed solution was under consistent mechanical stirring for 1 h until it changed into dark black. Where after, the product was collected by centrifugation and washed with water and ethanol alternately. Finally, the black slurry was dispersed in 5 mL ultrapure water and stored in a refrigerator under 4 ^oC when not in use.

1.6 Fabrication of ECL Biosensor.

Firstly, a batch of glassy carbon electrodes (GCE, Φ = 4 mm) were polished on chamois carefully with 0.3 and 0.05 μm alumina powder, and further cleaned through ultrasonic rinse with ultrapure water and absolute ethyl alcohol respectively. Later, 10 μL of L-M@MnO_x MFs suspension was dripped on the well-pretreated electrodes, drying at indoor temperature naturally. Soon afterwards, 10 μL of chitosan (0.5%) was dropped on the surface of the modified electrodes and left to dry in air. As well, 10 μL of AgPt NPs was decorated sequentially in the same way. Next, 10 μL of 1 μM H1 was incubated onto the electrodes overnight in refrigerator at 4 ^oC. Rinsed by phosphate buffer solution (PBS, 0.1 M, pH 7.4) to discard the uncombined DNA hairpins, the decorated GCEs were immersed in 1 mM 1-hexanethiol (HT) for 40 min to seal the remaining active sites of AgPt NPs.

1.7 Measurement Procedure.

10 μL of microRNA-21 (miRNA-21) solutions of varied concentrations were incubated on the developed biosensors at 37 °C for 30 min to hybridize with H1. After that, the modified biosensors were washed with PBS (pH 7.4) to remove excessive miRNA-21, then 10 μL of reaction solution containing 500 nM H1, 500 nM H2, 500 nM H3 and 500 nM H4 was incubated onto the surface to perform hybridization chain reaction (HCR) at 37 °C for 2.5 h to produce dendritic DNA nanostructures, and later unreacted hairpins were rinsed and removed with PBS. Afterwards, 10 μL aliquot of prepared Dox-FcCOOH compound was introduced to insert into the double helix structure of the generated dendritic DNA nanostructures. In the end, the assembled biosensors were rinsed in PBS (pH 7.4), and the ECL detection was carried out in 2 mL PBS (0.1 M, pH 8.0) on a MPI-A ECL analyzer under cyclic voltammetry scan from -1 V to 0.6 V. The photomultiplier voltage was set at 800 V, and the scan rate was 100 mV/s.

2. Results and Discussion

2.1 Morphology Characterization of Prepared Materials.

SEM images of MnO_x MFs and MWCNTs-COOH, TEM images of MWCNTs@MnO_x MFs (M@MnO_x MFs) were showed in Fig. S1. XPS patterns of M@MnO_x MFs were exhibited in Fig. S2. XRD patterns, HRTEM and SAED images were displayed in Fig. S3.

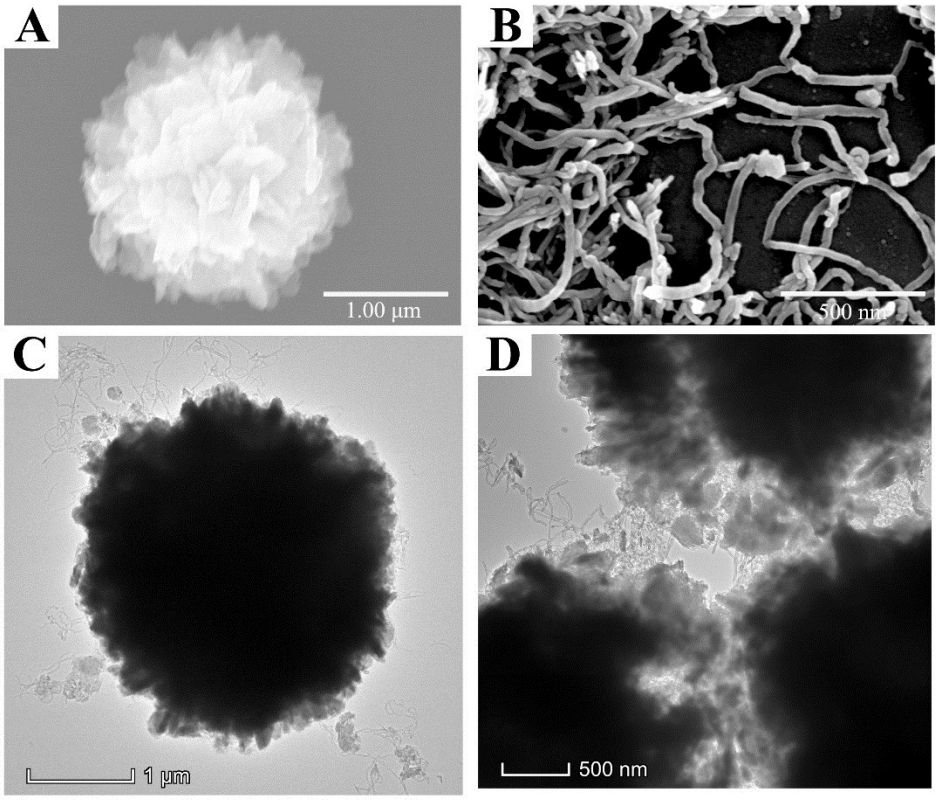

Fig. S1. SEM images of (A) MnO_x MFs and (B) MWCNTs-COOH, (C) TEM images of M@MnO_x MFs, (D) magnified image of Fig. 1B.

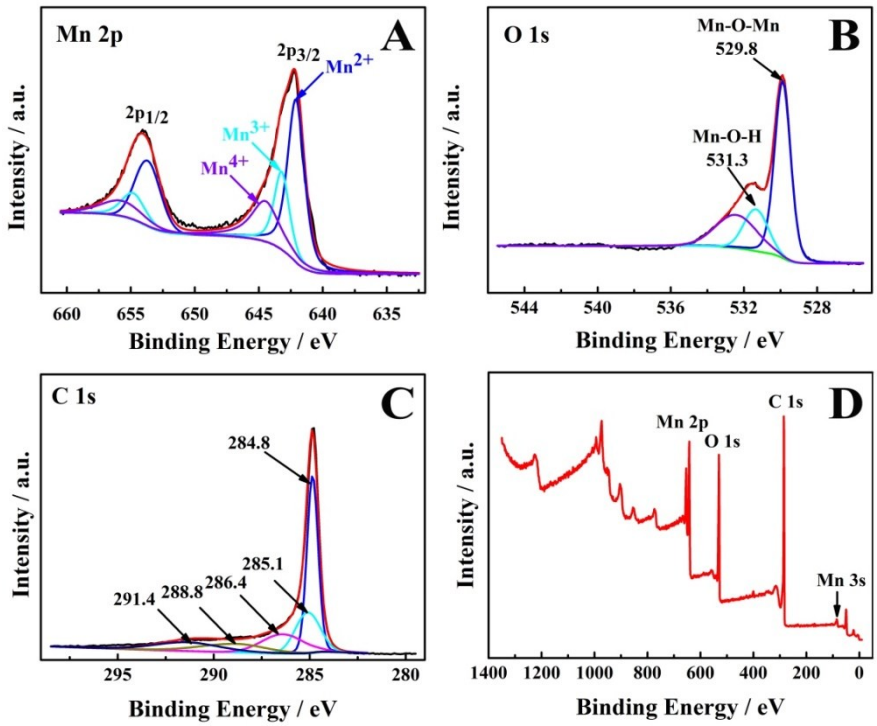

Fig. S2. XPS patterns of (A) Mn 2p, (B) O 1s, (C) C 1s and (D) full region of the M@MnO_x MFs.

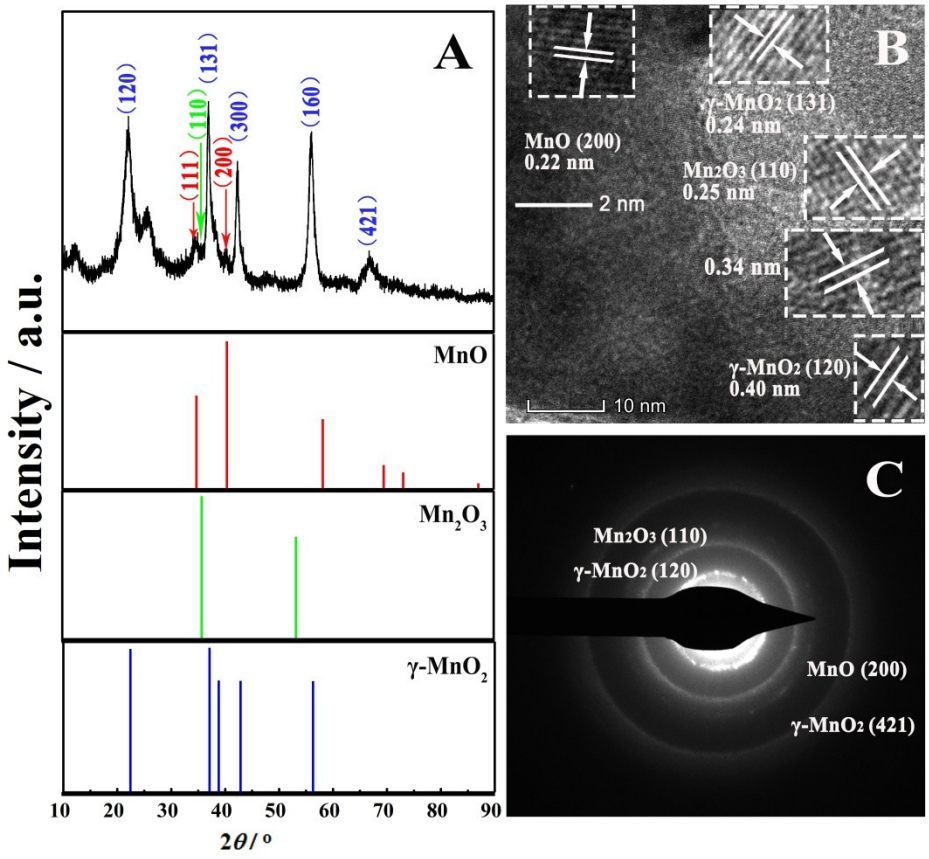

Fig. S3. (A) XRD patterns (MnO JCPDS 72-1533, Mn_2O_3 JCPDS 33-0900 and γ-MnO_2 JPCDS 14-0644), (B) HRTEM image and (C) SAED image of the M@MnO_x MFs.

The morphologies of AgPt NPs were characterized by SEM. In Fig. S4, AgPt NPs were mono-disperse sphere-like nanoparticles, the diameters of which were in the range of 30 ~ 80 nm.

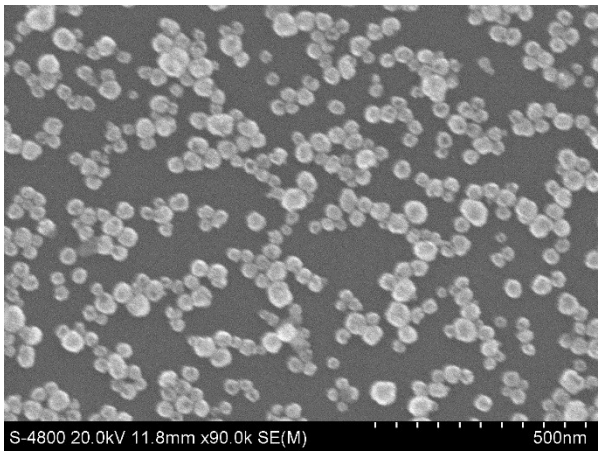

Fig. S4. SEM images of AgPt NPs.

2.2 Spectra Characterization of L-M@MnO$_x$ MFs Composite.

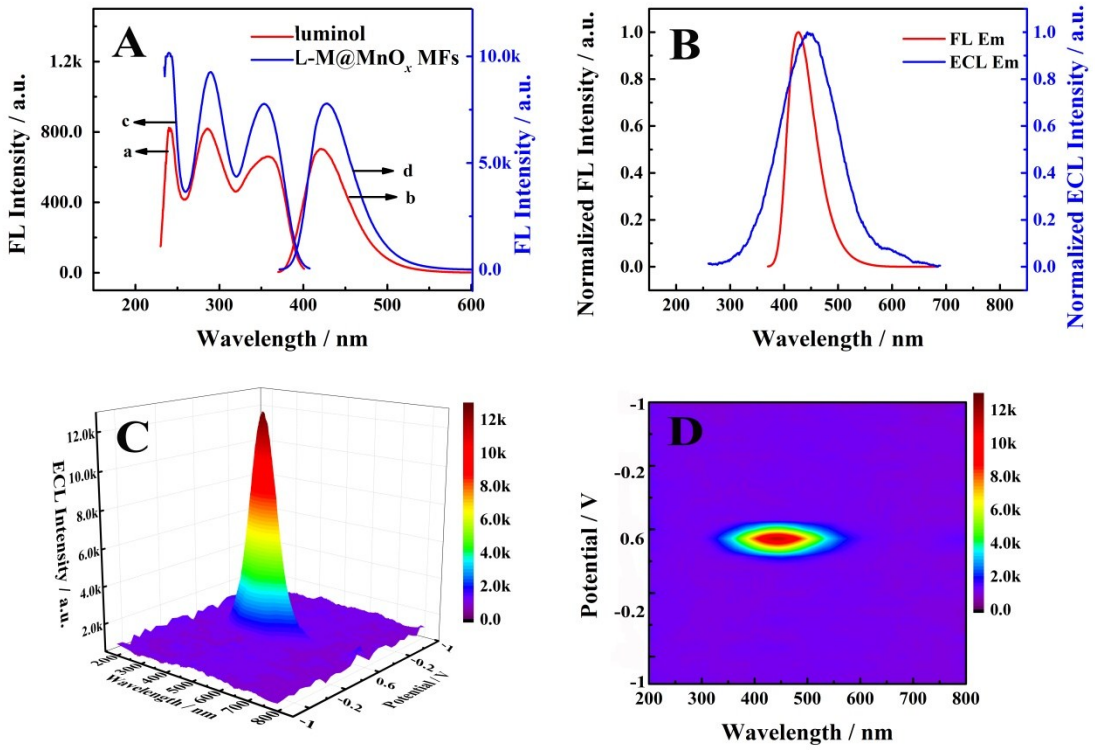

Fig. S5. (A) Fluorescence (a) excitation and (b) emission spectra of luminol, fluorescence (c) excitation and (d) emission spectra of L-M@MnO$_x$ MFs, (B) normalized fluorescence emission spectrum (λ_{ex} = 352 nm) and ECL emission spectrum of L-M@MnO$_x$ MFs, (C) 3D color map image and (D) planar heat map image of ECL emission of L-M@MnO$_x$ MFs.

2.3 Spectra Characterization of Luminol-MWCNTs@MnO_x MFs (L-M@MnO_x MFs) and Dox-FcCOOH Compound.

To confirm the synthesis of L-M@MnO_x MFs, the ultraviolet-visible (UV-vis) absorption spectra of MWCNTs, luminol and L-M@MnO_x MFs were investigated. As exhibited in Fig. S6A, MWCNTs-COOH (curve a) showed a weak and wide absorption band centered at 242 nm[4] related to 1D van Hove singularities.[5] Three characteristic absorption peaks could be observed both on the spectra of luminol (curve b) and L-M@MnO_x MFs (curve c), and a weak shoulder peak appeared at around 245 nm on curve c was related to MWCNTs-COOH, suggesting the successful synthesis of L-M@MnO_x MFs composite.[6] The minor shifts of peaks' position could be ascribed to the amide reaction.

The Dox-FcCOOH compound was characterized by UV-vis spectra (Fig. S6B). Clearly, Dox (curve a) had a wide characterized absorption band centered at 488 nm and a sharp peak at 233 nm ascribed to its amino group.[7] And obviously, two specific absorption peaks of FcCOOH (curve b) were located at 258 nm and 446 nm. After reacting with FcCOOH, the amino group absorption of Dox disappeared (curve c), demonstrating the consumption of amino in the synthesis process, which certified the successful preparation of Dox-FcCOOH compound. To further affirm the successful synthesis of Dox-FcCOOH, FTIR spectrum was applied to analyze the functional groups in Dox, FcCOOH and Dox-FcCOOH (Fig. S6C). In the spectrum of Dox (curve a), a strong peak at 3325 cm^{-1} was ascribed to the stretching vibration of N-H,

and a double peak containing 1616 cm^{-1} and 1583 cm^{-1} belonged to the bending vibration of N-H from the primary amine in Dox. Two peaks at 1729 cm^{-1} and 1285 cm^{-1} were assigned to the stretching vibration of C=O and C-N respectively. In the FTIR spectrum of FcCOOH (curve b), a sharp peak at 1655 cm^{-1} was attributed to the carbonyl (C=O) stretching vibration. As for Dox-FcCOOH (curve c), a strong single peak centered at 3415 cm^{-1} and a single peak at 1569 cm^{-1} were attributed the stretching vibration and bending vibration of N-H respectively, which indicated the secondary amide in Dox-FcCOOH and certified the successful amide reaction between Dox and FcCOOH. Besides, two absorption peaks at 1709 cm^{-1} and 1643 cm^{-1} were corresponding to C=O stretching vibration from the aliphatic ketone and secondary amide respectively. Meanwhile, a single peak at 1224 cm^{-1} was caused by the stretching vibration of C-N from secondary amide. Therefore, the FTIR spectra demonstrated the successful synthesis of Dox-FcCOOH.

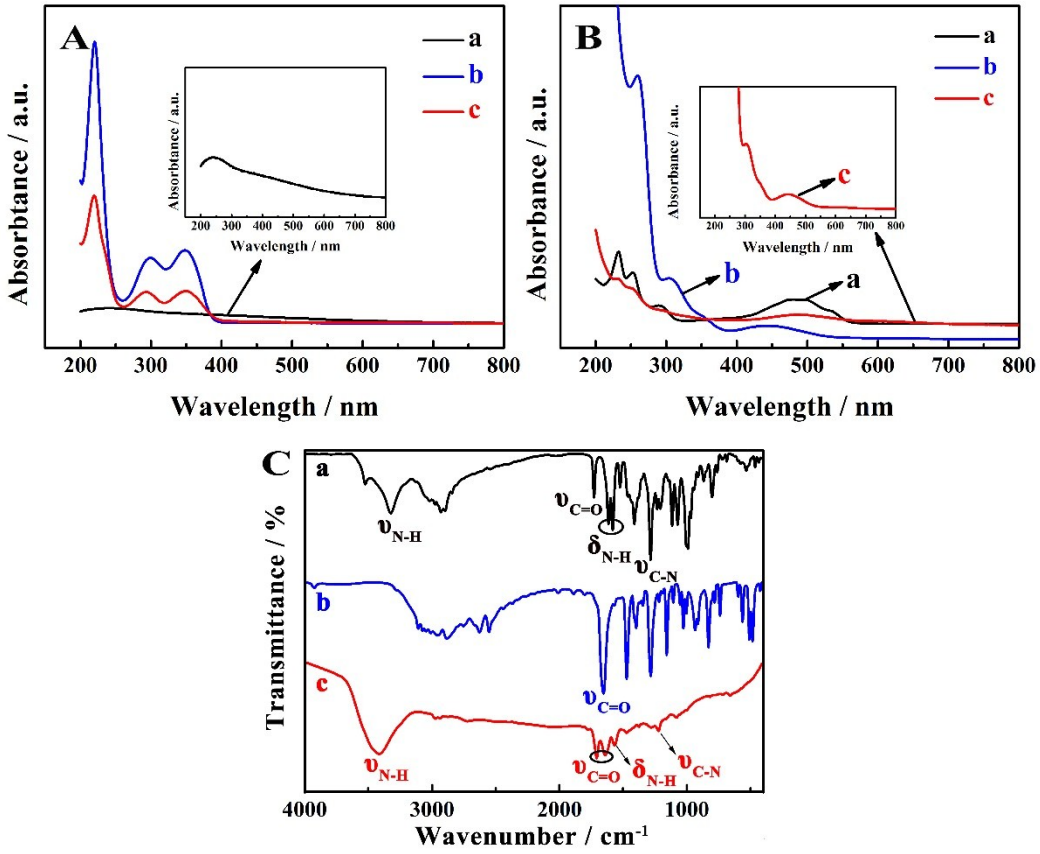

Fig. S6. (A) UV-vis absorption spectra of (a) MWCNTs-COOH, (b) luminol and (c) L-M@MnO_x MFs. (B) UV-vis absorption spectra of (a) Dox, (b) FcCOOH and (c) Dox-FcCOOH. (C) FTIR spectra of (a) Dox, (b) FcCOOH and (c) Dox-FcCOOH.

2.4 Possible Mechanism of the Proposed Ternary System.

Possible mechanism of the proposed ternary ECL system could be described as Fig. S7 and Scheme 1C (LH^- represented luminol anion, $L^{\bullet-}$ represented luminol anionic radicals, AP^{2-*} represented excited-state species 3-aminophthalate). First, luminol underwent a process of deprotonation and transformed to LH^-. Under potential scanning, LH^- was oxidized to $L^{\bullet-}$ via electro-oxidization (eq 1). In the presence of dissolved oxygen, $L^{\bullet-}$ could react with O_2 to produce a small amount of

$O_2^{\bullet-}$ (eq 2).[8] Meanwhile, dissolved oxygen could be reduced to HOO^- at about -0.65 V by a negatively potential scanning, which further became $O_2^{\bullet-}$ through positive scanning (eq 3~4).[9] And then $L^{\bullet-}$ was oxidized by $O_2^{\bullet-}$ to generate AP^{2-*} (eq 7), followed by an ECL emission process (eq 8). In the luminol/dissolved oxygen/MnO_x MFs system, the generation of HOO^- could be significantly accelerated (eq 3), therefore, more $O_2^{\bullet-}$ could accumulate to react with AP^{2-*} and exhibited an enhanced ECL emission. Also, the disproportionation reaction of $O_2^{\bullet-}$ to H_2O_2 and O_2 was also promoted in the ternary system (eq 5).[10] As a result, local oxygen concentration was enhanced to facilitate the reactions of eq 2 and eq 3. The decomposition rate of H_2O_2 to generate $OH^{\bullet}$ and $OH^{\bullet-}$ was also promoted by MnO_x MFs,[1] which played an important part in the deprotonation process of luminol and boosted the reaction speed of eq 1. Consequently, ECL signal from the ternary system was highly improved.

$$LH^- - e^- \longrightarrow LH^{\bullet} \longrightarrow L^{\bullet-} + H^+ \quad (1)$$

$$L^{\bullet-} + O_2 \longrightarrow O_2^{\bullet-} + L \quad (2)$$

$$O_2 + H_2O + 2e^- \xrightarrow{MnO_x\ MFs} HOO^- + OH^- \quad (3)$$

$$HOO^- - e^- \longrightarrow HOO^{\bullet} \longleftrightarrow O_2^{\bullet-} + H^+ \quad (4)$$

$$2O_2^{\bullet-} + 2H^+ \xrightarrow{MnO_x\ MFs} H_2O_2 + O_2 \quad (5)$$

$$H_2O_2 + e^- \xrightarrow{MnO_x\ MFs} OH^{\bullet} + OH^- \quad (6)$$

$$L^{\bullet-} + O_2^{\bullet-} \longrightarrow LO_2^{2-} \longrightarrow AP^{2-*} + N_2 \quad (7)$$

$$AP^{2-*} \longrightarrow AP^{2-} + h\nu \quad (8)$$

Fig. S7 Possible mechanism of the proposed ternary ECL system.

2.5 PAGE Characterization of Different DNA Samples.

As showed in Fig. S8, the four hairpins (H1, H2, H3, H4) with low molecular weight moved quickly during electrophoresis and emerged as bright bands in the bottom of lane 1 ~ 4 respectively. By contrast, through the hybridization chain reaction (HCR) between four hairpins and target miRNA-21, the products presented numerous new ladder-like bands in the upper side of lane 5, indicating the HCR products possessed high molecular weigh, which verified the fulfillment of HCR to prepare dendritic DNA nanostructures.

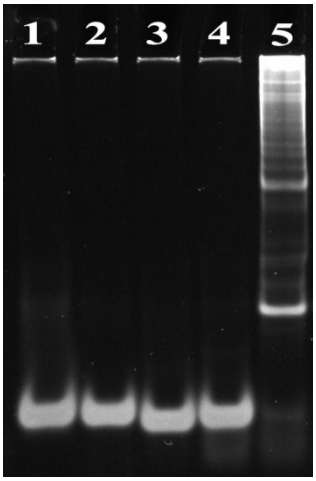

Fig. S8. Gel electrophoresis analysis of different samples: lane 1 ~ lane 4, H1 ~ H4 (1 μM); lane 5, miRNA-21 (1 μM) + H1 (1 μM), H2 (1 μM), H3 (1 μM) and H4 (1 μM).

2.6 Characterization of the ECL Biosensor.

To demonstrate the successful construction of the proposed biosensor, cyclic voltammetry (CV) curves were recorded stepwise after each modification

implemented on the electrodes. As portrayed in Fig. S8, the L-M@MnO_x MFs modified GCE (curve b) exhibited decreased redox peak currents of $[Fe(CN)_6]^{3-/4-}$ comparing with the bare GCE (curve a) because of the poor conductivity of manganese oxides, while a notable oxidation peak at 0.56 V occurred, which was assigned to the oxidation reaction of luminol. When chitosan was incubated on the modified GCE (curve c), the current further declined due to the fact that chitosan is a sort of non-conductive polymer hampering the electron transfer between solution and electrode surface. Afterwards, the addition of AgPt NPs gave rise to a remarkable enhancement of current (curve d) as a result of its excellent conductivity. Then, H1 (curve e), HT (curve f) and miRNA-21 (curve g) were successively decorated on the GCE, and consequently consecutive diminutions of the redox peak currents were observed, which could be explained by steric hindrance effect and electrostatic repulsion. After that, further reduction occurred on account of the formation of the negatively charged DNA nanostructures (curve h). Furthermore, as the import of the Dox-FcCOOH compound lead to an incremental steric hindrance, an even more flat cyclic voltammetry curve was obtained (curve i).

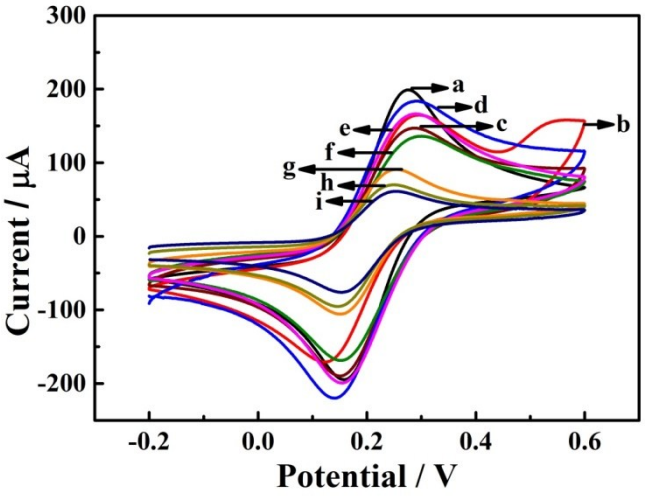

Fig. S9. CV characterization performed in 2 mL PBS (pH 7.4) containing 5 mM $[Fe(CN)_6]^{3-/4-}$: (a) bare GCE, (b) L-M@MnO_x MFs/GCE, (c) chitosan/L-M@MnO_x MFs/GCE, (d) AgPt NPs/chitosan/L-M@MnO_x MFs/GCE, (e) H1/AgPt NPs/chitosan/L-M@MnO_x MFs/GCE, (f) HT/H1/AgPt NPs/chitosan/L-M@MnO_x MFs/GCE, (g) miRNA-21 (1 pM) /HT/H1/AgPt NPs/chitosan/L-M@MnO_x MFs/GCE, (h) DNA nanostructures /HT/H1/AgPt NPs/chitosan/L-M@MnO_x MFs/GCE, (i) Dox-FcCOOH/DNA nanostructures/HT/H1/AgPt NPs/chitosan/L-M@MnO_x MFs/GCE.

2.7 Optimization of the Experimental Conditions

For the sake of exploring the optimal detection conditions, the duration of HCR and intercalating reaction between Dox-FcCOOH and the generated dendritic DNA nanostructures were investigated. As showed in Fig. S10A, in the condition of identical else parameters (100 pM miRNA-21, Dox-FcCOOH incubated for 2 h), with the extension of the hybridization time from 0.5 h to 2.5 h, the ECL intensity plummeted down obviously. While the reaction time of HCR was over 2.5 h, the

ECL intensity reduced at a mild rate. Hence, 2.5 h was chosen as the suitable hybridization time length. As to the appropriate duration for the Dox-FcCOOH compound to intercalate into the dendritic DNA nanostructures, the same remaining experimental conditions were controlled (100 pM target miRNA-21, 2.5 h for HCR) to study the influence of intercalating duration. It could be recognized from Fig. S10B that when the reaction between Dox and DNA nanostructures lasted for more than 3h, the ECL intensity dwindled more sluggishly than before. Therefore 3 h was taken as the modest time duration in the following tests.

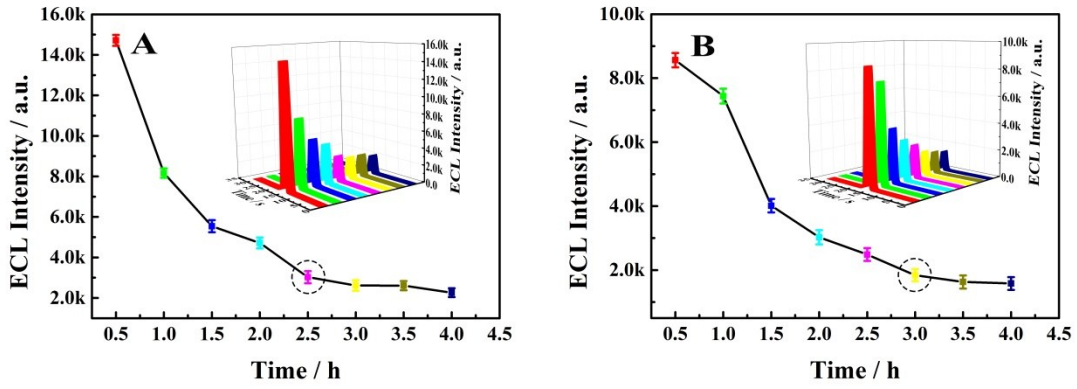

Fig. S10. Optimization on the duration of (A) HCR and (B) the intercalating reaction between Dox-FcCOOH and the generated dendritic DNA nanostructures.

2.8 Selectivity and Stability of the Proposed Biosensor.

In order to evaluate the selectivity of the biosensor, miRNA-let-7a (10 nM), miRNA-141 (10 nM) and miRNA-155 (10 nM) were used as interference substances. As seen in Fig. S11A, when target miRNA-21 was replaced by the interfering miRNAs respectively, there were almost no obvious changes in the ECL signal versus

the blank assay (replacing miRNA-21 with PBS), verifying the constructed biosensor had no distinct response to those interfering miRNAs. Moreover, when a mixture solution (containing 100 pM miRNA-21, 10 nM miRNA-let-7a, 10 nM miRNA-141 and 10 nM miRNA-155) was incubated on the biosensor to trigger the HCR, a similar ECL intensity was gained with only a little difference from that of the biosensor with miRNA-21 (100 pM), which suggested the coexistence of those nonspecific miRNAs caused no perceptible effects on the analysis of miRNA-21. Based on the above results, the fabricated biosensor exhibited fantastic selectivity and specificity to the target miRNA-21.

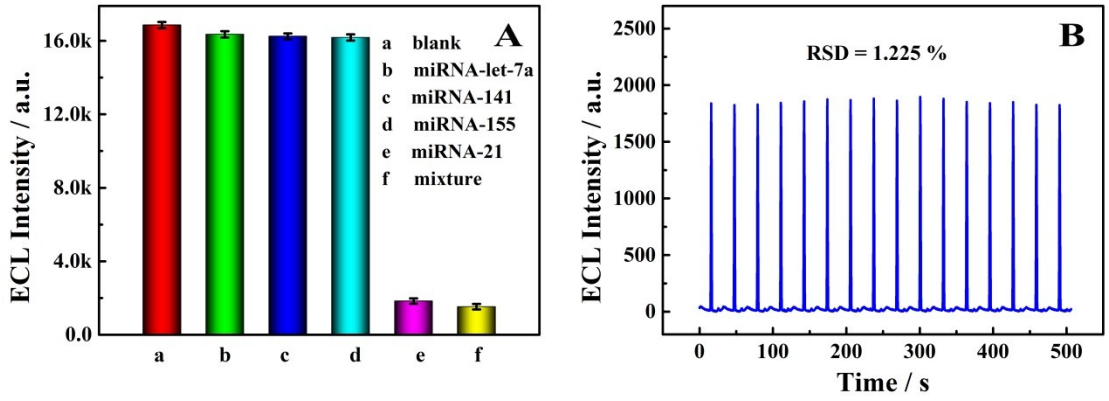

Fig. S11. (A) Selectivity of the designed biosensor for the detection of miRNA (100 pM) comparing with three interfering miRNAs (10 nM), and (B) stability of the developed biosensor under 16 cycles of potential scan (-1 ~ 0.6 V) in PBS (pH 8.0) with 100 pM miRNA-21.

The stability of the biosensor was assessed by continuous cyclic potential scan under the detection conditions. As delineated in Fig. S11B, the biosensor incubated with 100 pM miRNA-21 emitted nearly unaltered ECL intensity after 16 cycles (R.S.D. =1.225%), which demonstrated that the developed biosensor possessed

excellent stability.

2.9 Performance of the Designed Biosensor in Tumor Cell Analysis.

To check out the practicability and validity of the proposed biosensor, MCF-7 (human breast cancer cell) extract, which was acquired through disposing a known amount of cells with a RNA extraction kit, was made use of to measure the ECL response towards it. In Fig. S12A, the ECL signal declined as the quantity of cells accumulated. Moreover, the ECL intensity diminution (ΔI_{ECL}) showed a significant linear correlation with the logarithm of the number of cells (lg$N$), with the calibration equation expressed as ΔI = -1478.8 + 2419.09 lg$N$ (Fig. S12B). Therefore, these results showed that the developed miRNA biosensor possessed a favorable prospect in practical detection.

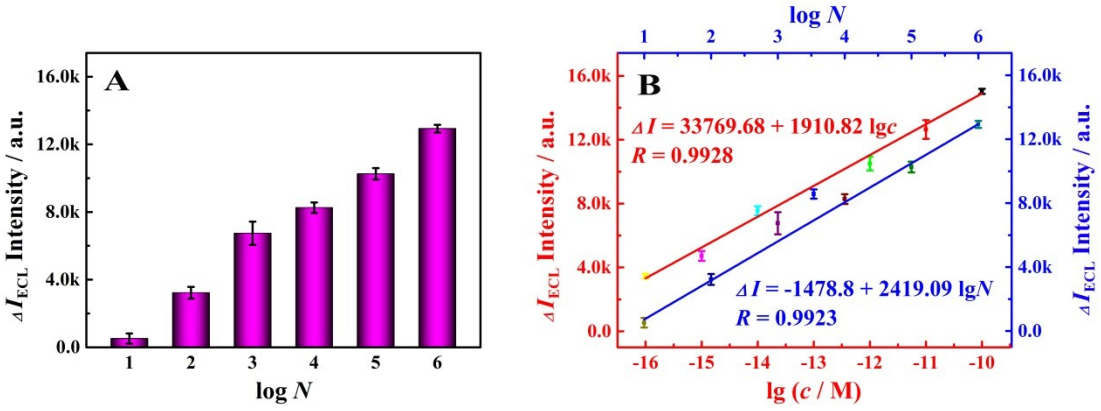

Fig. S12. Application of the fabricated biosensor in the lysate of MCF-7cells.

Table S2. Comparison of other methods and this work for miRNA detection.

detection method	target	dynamic range	detection limit	reference

fluorescence	miRNA-27a	1 pM ~ 1 nM	0.8 pM	11
fluorescence	miRNA-21	10 fM ~ 1 nM	5.7 fM	12
electrochemistry	miRNA-16	0.1 pM ~ 100 nM	16 fM	13
PEC	miRNA-141	1 fM ~ 10 pM	0.5 fM	14
ECL	miRNA-21	10 fM ~ 0.1 nM	6.6 fM	15
ECL	miRNA-107	1.0 fM ~ 1.0 nM	1 fM	16
ECL	miRNA-21	100 aM ~ 100 pM	10.7 aM	This work

References

1. C. C. Wang, J. L. Fu, Y. Zhang, H. Zhao, X. Wei and R. J. Zhang, *Chem. Commun.,* 2018, **54**, 7330−7333.
2. X. J. Su, H. Q. Li, X. J. Lai, Z. P. Yang, Z. H. Chen, W. J. Wu and X. R. Zeng, *J. Mater. Chem. A,* 2018, **6**, 16910–16919.
3. Y. H. Zhang, J. J. Li, H. Rong, X. W. Tong and Z. H. Wang, *Langmuir,* 2017, **33**, 5991–5997.
4. S. S. Baghbaderani, A. Noorbakhsh, *Biosens. Bioelectron.,* 2019, **131**, 1–8.
5. Z. L. Han, F. Li, J. N. Shu, L. F. Gao, X. Y. Liu and H. Cui, *ACS Appl. Mater. Interfaces,* 2016, **8**, 17454−17460.
6. H. Ke, X. Zhang, C. S. Huang and N. Q. Jia, *Biosens. Bioelectron.,* 2018, **103**, 62–68.
7. F. F. Wu, Y. Zhou, H. Zhang, R. Yuan and Y. Q. Chai, *Anal. Chem.,* 2018, **90**, 2263−2270.
8. H. Cui, G. Z. Zou and X. Q. Lin, *Anal. Chem.,* 2003, **75,** 324−331.
9. Q. H. Xu, J. L. Liang, X. Teng, X. Yue, M. Lei, C. F. Ding and C. Lu. *Chem. Commun.,* 2019, **55,** 5563−5566.
10. D. N. Zhang, S. W. Yan and W. H Song, *Environ. Sci. Technol.,* 2014, **48,** 12645−12653.
11. D. Zhu, B. Lu, Y. Zhu, Z. H. Ma, Y. Q. Wei, S. Su, L. H. Wang, S. P. Song, Y. Zhu, L. H. Wang and J. Chao, *ACS Appl. Mater. Interfaces,* 2019, **11**, 11220−11226.
12. K. Y. Zhang, S. T. Song, L. Yang, Q. H. Min, X. C. Wu and J. J. Zhu, *Chem. Commun.,* 2018, **54**, 13131−13134.
13. H. R. Tang, J. H. Zhu, D. M. Wang and Y. X. Li, *Biosens. Bioelectron.,* 2019, **131**, 88−94.

14. N. Zhang, X. M. Shi, H. Q. Guo, X. Z. Zhao, W. W. Zhao, J. J. Xu and H. Y. Chen, *Anal. Chem.,* 2018**, 90**, 11892−11898.

15. P. Zhang, J. Jiang, R. Yuan, Y. Zhuo and Y. Q. Chai, *J. Am. Chem. Soc.,* 2018, **140**, 9361−9364.

16. X. L. Huo, H. Yang, W. Zhao, J. J. Xu and H. Y. Chen, *ACS Appl. Mater. Interfaces,* 2017, **9**, 33360−33367.